An Experimental Study on the Performance of Check Valve-Aided Savonius Wind Rotors with Semi-Circular Blade

Ivan Farozan[1*], Yuli Setyo Indartono[1,2]

[1]*Faculty of Mechanical and Aerospace Engineering, Institut Teknologi Bandung, Bandung 40132, Indonesia*
[2]*Research Center for New and Renewable Energy, Institut Teknologi Bandung, Bandung 40132, Indonesia*

Abstract. The Savonius wind turbine is perceived favorable for a small-scale application because it is simple, relatively inexpensive, insensitive to wind directions, and has a good self-starting ability. However, it has a low power coefficient caused by the negative torque from the returning blade. This study aimed to investigate the effect of valve addition on the semi-circular Savonius rotor's performance. The experiments for this study were conducted on an open jet wind tunnel, with the valve located near the rotation axis, blade center, and rotor tip. The valve opening area ratio used was 0.02, 0.04, and 0.06, with Reynolds numbers 73,000, 86,000, and 99,000. The results showed that rotors with a valve placed near the tip performed better than those at the blade center and near the rotation axis. The performance decreased with an increase in the valve opening area ratio. Furthermore, the performance-improvement magnitude decreased with an increase in the Reynolds number. The rotor with a single valve near the tip performed the highest at a Reynolds number of 73,000. It achieved a maximum power coefficient of 0.199 compared to 0.183 obtained by a conventional Savonius rotor.

Keywords: Augmentation; Check valve; Renewable energy; Savonius wind-rotor; Wind turbine

1.   Introduction

The Intergovernmental Panel on Climate Change (IPCC) warned that the world would reach 1.5 °C of warming by 2040, and only swift and drastic cuts in carbon emissions would help prevent an environmental disaster (IPCC, 2022). One way to reduce carbon emissions is reduced by using renewable energy sources such as wind energy to decarbonize the global electricity generation systems. In 2019, global wind power capacity reached 651 GW, contributing approximately 5.9% of global electricity generation (REN21, 2019). With wind energy costs expected to drop significantly in the future, this contribution is expected to increase (Wiser *et al.,* 2021).

Savonius rotor is a vertical axis wind turbine (VAWT) comprising two semi-circular buckets arranged asymmetrically to resemble an 'S' shape. It works based on drag force with a slight contribution from the lift force (Alom, Borah, and Saha, 2018). The positive torque generated by an advancing blade moving with the wind is higher than the negative torque generated by the returning blade moving against the wind. The difference between the two torques causes the rotor to spin. The Savonius rotor power coefficient (C_P) is much lower than the horizontal axis wind turbine (HAWT) due to the negative torque produced.

However, it has several intrinsic advantages over the HAWT, such as simpler design, good starting ability, omnidirectional, lower noise, and easier to maintain (Kumar, Raahemifar, and Fung, 2018). These advantages make the rotor more suitable for harnessing wind power in urban sites, building rooftops, and remote areas (Mao *et al.*, 2020; Ishugah *et al.*, 2014; Cho, Jeong, and Sari, 2011). In addition to energy generation, wind turbines installed in an urban area allow direct use of energy which eliminates energy transmission losses (Krasniqi, Dimitrieska, and Lajqi, 2022). When combined with a suitable and improved generator design, such as a reduced cogging-torque permanent magnet generator (Nur and Siregar, 2020), the Savonius rotor may provide an interesting method for small-scale wind power generation. The basic geometry of a conventional Savonius rotor is illustrated in Figure 1.
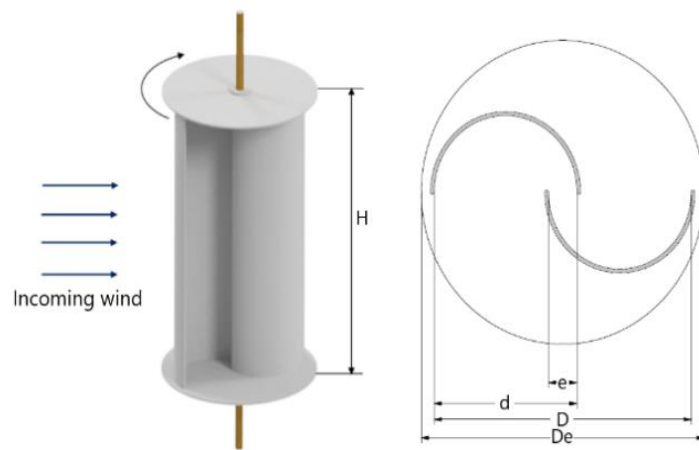

Figure 1 Basic geometry of a conventional Savonius rotor

The performance of a Savonius rotor highly depends on its geometric parameters. Saad *et al.* (2020) found that the rotor with end plates performed better, with the optimum value for end plate diameter (De) at 1.1 of the rotor diameter (D). Mahmoud *et al.* (2012) investigated the aspect ratio (AR), a non-dimensional parameter resulting from dividing the rotor height (H) by its diameter. The study found that the maximum C_P (C_{PMax}) was improved as the AR increased. Saad, Ookawara, and Ahmed (2022) observed a similar finding on multi-stage rotors. This C_P improvement for a higher AR reduces loss at the tip, similar to adding end plates (Akwa, Vielmo, and Petry, 2012). Studies on the overlap ratio (β) of the distance between rotor blades (e) and the blade chord length (d) found that the optimum value ranges from 0.15 to 0.2 (Cuevas-Carvajal *et al.*, 2022; Alom and Saha, 2017; Roy and Saha, 2013). Additionally, Kamoji, Kedare, and Prabhu (2009) investigated the effect of the Reynolds number on a conventional and modified Savonius rotor. The study found that the C_{PMax} improved by 19% as the Reynolds number increased from 80,000 to 150,000.

The modification f the conventional Savonius rotor blade shape can also improve its performance. Abdelaziz *et al.* (2022) numerically studied the performance of a conventional Savonius rotor with various outer and inner arc angles and gap ratios. They managed to improve the C_{PMax} by 4.5% and 12.9% with a 160⁰ outer angle and 20⁰ inner angle, respectively. A novel Savonius rotor with a modified-bach blade was proposed by Elmekawy, Saeed, and Kassab (2021). They found a 32.2% C_{PMax} improvement over a conventional Savonius rotor through numerical study. The blade shape was also modified to improve the Savonius performance at a higher TSR range (above 0.8). Savonius rotor

with a combination of the semi-circular and elliptical profile was found to have C_{PMax} at TSR=1.4, double that of a conventional rotor's TSR=0.7 (Le *et al.,* 2022). Based on the result, Dinh Le, Minh, and Trinh (2022) further modified the previous rotor into a combination of multi-curve and auxiliary blades. The new rotor combination not only possessed a higher C_{PMax} at a higher TSR, but it also exhibited a 6.9% higher C_P than the conventional rotor in the lower TSR range.

Several studies have suggested different methods to enhance the performance of the Savonius rotor. For instance, Mohamed *et al.* (2010) improved the CP by 27.3% by placing a deflector upstream to prevent the wind from hitting the returning blade. Nimvari, Fatahian, and Fatahian (2020) used a porous deflector and achieved a 10% increase in C_{PMax}. El-Askary *et al.* (2015) proposed a design that incorporated a Savonius rotor inside curved guide plates, which achieved a C_{PMax} of 0.52 at a TSR of 1.1. However, this design produced large wakes behind the rotor, which could affect the operation of other turbines in a wind farm. Although these methods significantly improve performance, they compromise the simplicity and omnidirectional nature of the Savonius rotor.

Ideal augmentation methods can improve rotor performance while keeping all the Savonius advantages intact. One of the methods is the addition of a check valve to the rotor blades. This method allows a portion of wind freestream to pass through the returning-blade convex side, reducing the drag force and lowering the negative torque. Furthermore, valve addition can be a complementary method with the potential to further enhance an already high-performance Savonius rotor with a modified blade.

Rajkumar and Saha (2006) first investigated the valve-addition method by placing slot-shaped aluminum hinged-type valves on a conventional and twisted Savonius rotor. Saha Thotla, and Maity (2008) later used a thin fabric called Rexine as the valve material instead of aluminum and conducted experiments using an open jet wind tunnel. The findings showed that the two-stage, valve-aided Savonius rotor had a 19% higher C_{PMax} than a conventional rotor. Both of the aforementioned studies used a fixed-size valve placed at the center of the blade. Amiri and Anbarsooz (2019) investigated the effect of valve location on a conventional Savonius rotor's performance. The study used a rectangular pivot-type valve made from the same material as the rotor. The valve's opening area ratio (OAR), which is the ratio between the area of the valves and the rotor's frontal area (D.H), was fixed at 0.33. This pivotal valve was placed near the rotation axis as well as in the middle and at the tip of the rotor. The results showed that the valve at the tip location yielded a 20.8% performance improvement. Furthermore, Borzuei, Moosavian, and Farajollahi (2021) performed a numerical experiment on the effect of adding a rectangular pivot-type valve to the static torque coefficient of a Savonius rotor with three blades. The results showed a 14.5% improvement in the static torque coefficient. This was indicated by the large pivot valve with an unlimited opening angle and counter-clockwise opening direction placed at the center of the rotor blade.

Previous studies have shown that using a part of the rotor blade as a pivot-type valve can have a positive effect (Borzuei, Moosavian, and Farajollahi, 2021; Amiri and Anbarsooz, 2019). However, a large OAR can have a negative impact on the structural integrity and manufacturability of the rotor. The slot-shaped hinge-type valve proposed by Saha, Thotla, and Maity (2008) has better structural integrity and manufacturability. However, previous studies on Savonius rotors with hinge-type valves did not investigate the effect of valve locations and OAR on the rotor's performance under different wind speeds. This study aims to fill this gap. Moreover, in contrast to the slot-shaped valve used in by Saha, Thotla, and Maity (2008) this study employs a circular valve to improve the manufacturability of the rotor blade.

2.   Methods

2.1. Studied Rotor Design and Manufacturing

This study investigated a single-stage Savonius with two semi-circular rotor blades. All the studied rotors have the same design and dimension. The valves were placed near the rotor rotation axis (A), at the center of the rotor blade (B), and near the rotor tip (C). Moreover, the study used three increasing OAR for each location to study ten rotors, including the non-valve-aided rotor. Tables 1 and 2 show the geometrical dimension and rotor specifications, while the valve location and arrangements are depicted in Figure 2a.

The rotors were manufactured using 3D printers and PLA+ material with a thickness of 2.5mm. Each rotor was divided into lower and top plates and rotor blades, a design chosen to reduce manufacturing time and material use while allowing for quick reconfiguration. The valve body was made from synthetic leather pasted onto the rotor blade. Figure 2b shows the manufactured rotors.

Table 1 Geometrical dimension of the studied Savonius semi-circular rotor

Chord length (d)	Rotor diameter (D)	End plate diameter (De)	Rotor Height (H)	Rotor Aspect ratio (AR)	Overlap ratio (β)
100 mm	180 mm	198 mm	360 mm	2	0.2

Table 2 Studied rotors identification and specification

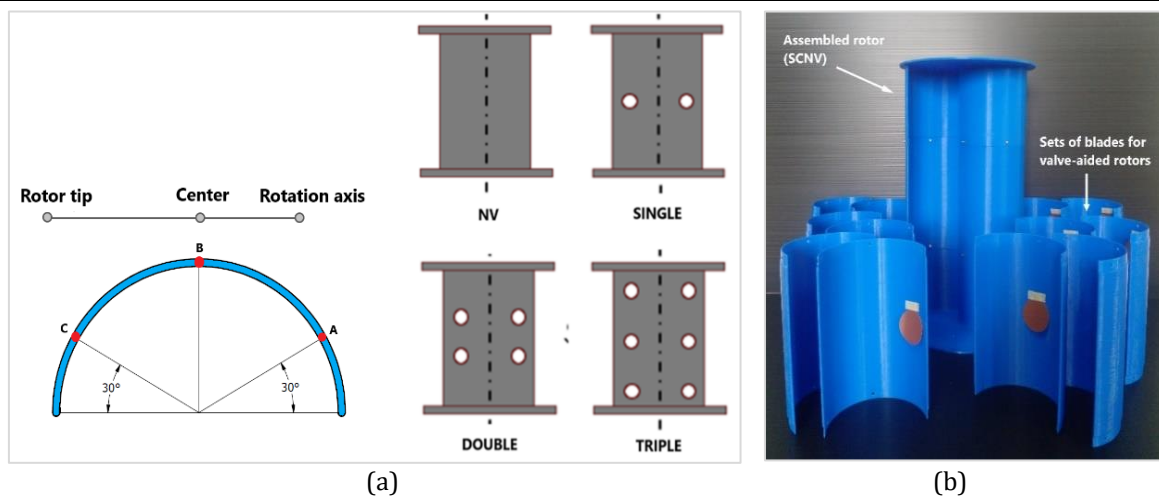| Parameter	Rotor Identification									
	SCNV	SCA1	SCA2	SCA3	SCB1	SCB2	SCB3	SCC1	SCC2	SCC3
Valve Location	N/A	Near the rotation axis			At the blade center			Near rotor tip		
Valve Qty	0	1	2	3	1	2	3	1	2	3
OAR	0	0.02	0.04	0.06	0.02	0.04	0.06	0.02	0.04	0.06

Figure 2 (a) Valve locations and arrangement on the rotor; (b) 3D printed rotors

2.2. Experimental Setup

The experiments were performed using the low-speed open jet wind tunnel at the Institut Teknologi Bandung. The wind velocity at the tunnel exit (V_∞) could be adjusted up to 10 m/s using a variable speed drive. The averaged wind velocity at the tunnel exit was measured using a calibrated hotwire anemometer. The experiments were conducted at a Reynolds number of 73,000, 86,000, and 99,000. The rotor axis was positioned 300 mm away from the wind tunnel exit. The open test section in which the rotor was situated measured 1,000 mm x 600 mm, resulting in a blockage ratio of 12%. This value is low for

an open-type wind tunnel test and does not require a blockage correction factor (Gonçalves, Pereira, and Sousa, 2022; Van Bussel *et al.,* 2004). The overall setup of the experimental study is depicted in Figure 3a.

The study used a DYN-200 rotary torque meter to measure the torque (T) and the rotor's rotation speed (N). The torque meters measurement was calibrated using known torques, while the rotation speed was checked against a calibrated optical tachometer. The meter accuracy was specified as ±0.1% and ±1 rpm for the torque and rotation speed, respectively. Furthermore, the torque meter output was connected to a laptop via a Labjack U6 data acquisition module. A hysteresis brake and a DC generator were combined to simulate a dynamic load. At each test point, measurements were taken at a sampling rate of 4 Hz for 15 seconds. Figure 3b shows the instrumental setup.
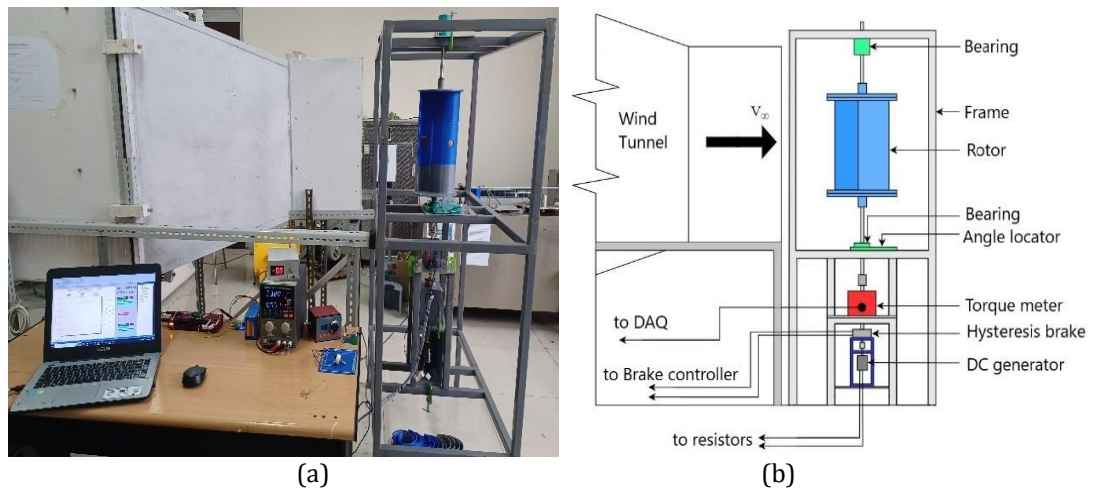

(a) (b)

Figure 3 (a) Overall experimental setup; (b) Instrumentation setup

2.3. Data Reduction

The study measured the freestream wind velocity (V_∞), rotor torque (T), and rotor rotational speed (N). The rotor was operated under a steady wind velocity and constant load during a dynamic test. The torque and rotation speeds were measured for a fixed time and then averaged. The load was then varied to obtain the rotor's performance characteristics. The torque loss due to bearing frictions cannot be ignored at higher rotational speeds. Therefore, a separate experiment was conducted to obtain the frictional power loss characteristic. The dimensionless rotor tip speed ratio (TSR) was then calculated using Equation 1:

$$TSR = \frac{\omega D}{2V_\infty} \tag{1}$$

where D is the rotor diameter (m), V_∞ is the wind velocity (m/s), and ω is the rotor angular velocity (rad/s) calculated using Equation 2:

$$\omega = \frac{2\pi N}{60} \tag{2}$$

where N is the measured rotor rotation speed (rpm). The dimensionless rotor power coefficient C_P is expressed using Equation 3:

$$C_P = C_T\,TSR \tag{3}$$

where TSR is the tip speed ratio given by Equation 1, and C_T is the dimensionless rotor torque coefficient calculated using Equation 4:

$$C_T = \frac{4T}{\rho V_\infty^2 HD^2} \tag{4}$$

where T is the measured torque (N.m), H is the rotor height (m), and ρ is the air density in (kg/m^3).

The uncertainty related to the measurement is calculated using the root-sum-square method (Wheeler and Ganji, 2009). The total uncertainties ($u_{\bar{x}}$) for the measured quantities (T, N, and V_∞) are calculated using Equation 5:

$$u_{\bar{x}} = \left(B_x^2 + P_{\bar{x}}^2\right)^{1/2} \tag{5}$$

where B_x is the systematic uncertainty taken from the instrument's accuracy specification, and $P_{\bar{x}}$ is the random uncertainty based on the standard deviation of the mean. The uncertainties for derived quantities (TSR, C_P, and C_T) are then calculated using the propagation of error method shown in Equation 6:

$$u_R = \left(\sum_{i=1}^{n}\left[u_{\bar{x}i}\frac{\partial R}{\partial x_i}\right]^2\right)^{1/2} \tag{6}$$

where u_R is the total uncertainty for the derived quantities, and $\frac{\partial R}{\partial x_i}$ is the sensitivity coefficient of derived quantities R with respect to variable x_i. The confidence level associated with the uncertainties was chosen at 95%. The total uncertainties for the TSR, C_T, and C_P are 2.3%, 4.0%, and 6.3% respectively.

3.   Results and Discussion

3.1. Conventional (Non-Valve-Aided) Savonius Rotor Performance

Figures 4a and 4b shows the power and torque coefficients of the conventional non-valve-aided Savonius rotors (SCNV) versus the tip speed ratio at different Reynolds numbers.. The results show a C_PMax of 0.183, 0.200, and 0.210 for Reynolds numbers 73,000, 86,000, and 99,000, respectively. The tip speed ratio corresponding to the C_PMax ranged from 0.84 to 0.86. This result supports previous studies that found a C_PMax range of 0.17 to 0.21 (Banerjee, 2019; Ferrari *et al.*, 2017; Roy and Saha, 2015; Torresi *et al.*, 2014).
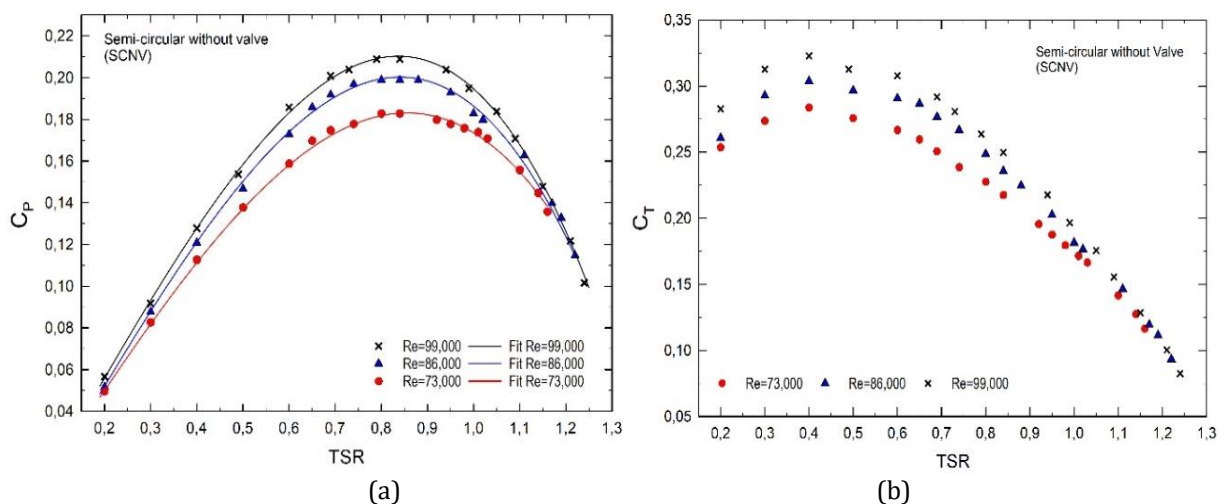

(a)   (b)

Figure 4 The effect of Reynolds number on the Savonius rotor (a) coefficient of power; and (b) coefficient of torque

The results suggest that the power coefficient increased as the Reynolds number increased. The C_PMax value increased by 14.6% as the Reynolds number increased from 73,000 to 99,000, which is consistent with the findings of Kamoji, Kedare, and Prabhu (2009). The increase in C_PMax was attributed to the delayed separations at the rotor blades at higher Reynolds numbers or wind velocities (Kamoji, Kedare, and Prabhu, 2009). Similarly, the C_TMax also increased with the Reynolds number. The C_TMax values for Reynolds numbers 73,000, 86,000, and 99,000 were 0.284, 0.304, and 0.323, respectively. The C_T

peaked at a tip speed ratio of 0.4 and decreased almost linearly as the tip speed ratio increased, which was observed for all three Reynolds numbers.

3.2. Effect of Valve Locations on the Rotor Performance

Three rotors were aided with a single valve (OAR = 0.02) placed at near the rotation axis (SCA1), at the blade center (SCB1), and at the rotor tip (SCC1). These rotors were tested to investigate the effect of valve locations on the rotor performance. The results for the power coefficient are depicted in Figures 5a, 5b, and 5c. Figures 5d, 5e, and 5f show the results for the torque coefficient.
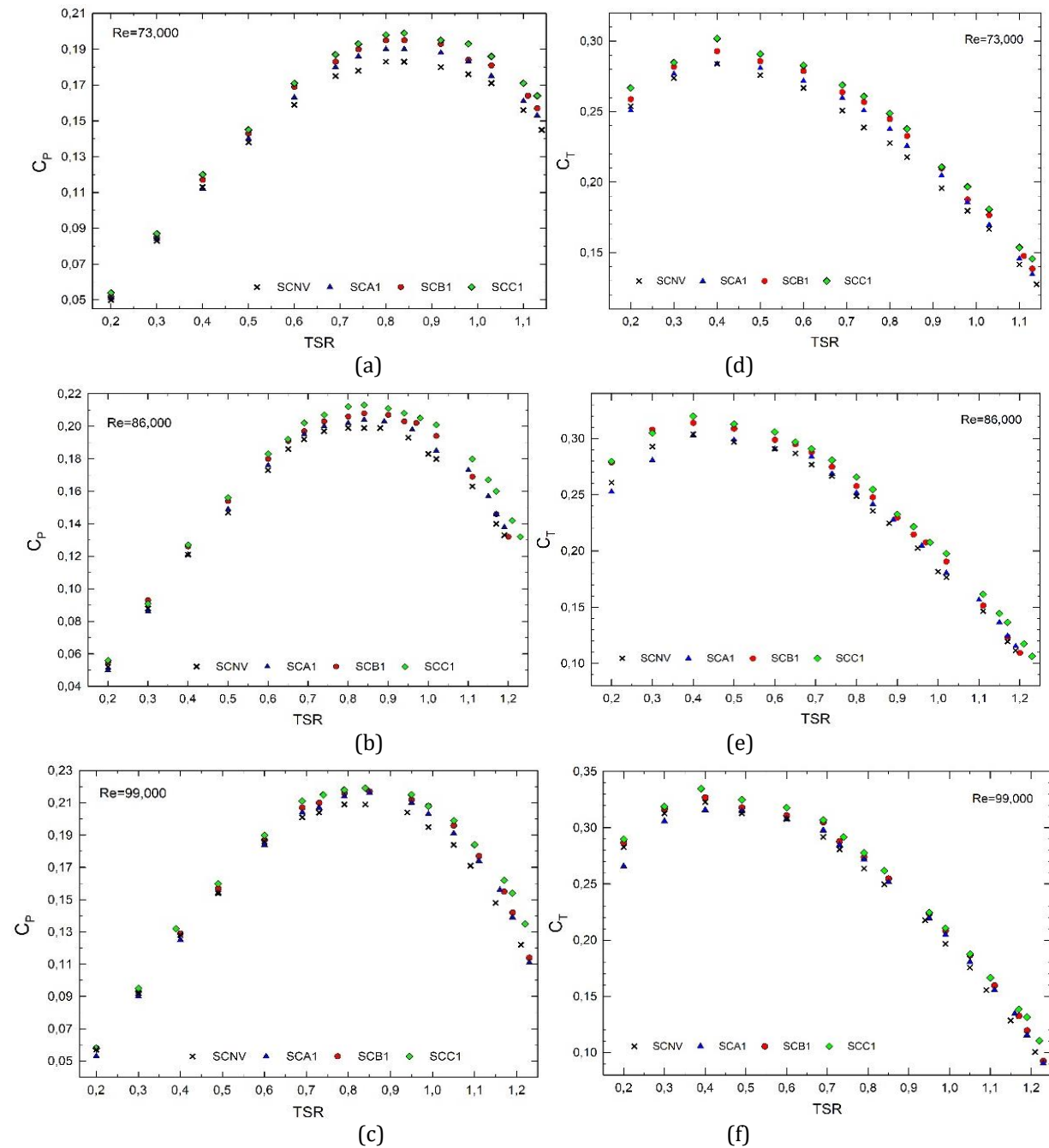

Figure 5 The effect of valve locations on SCNV, SCA1, SCB1, and SCC1 rotor (a) C_P vs TSR at Re=73,000; (b) C_P vs TSR at Re=86,000; (c) C_P vs TSR at Re=99,000; (d) C_T vs TSR at Re=73,000; (e) C_T vs TSR at Re=86,000; and (f) C_T vs TSR at Re=99,000

The rotors with a single valve performed better than the non-valve-aided (SCNV) rotors in all three locations and for all Reynolds numbers. However, the magnitude of C_{PMax} improvement decreased as the Reynolds number increased. For instance, the SCC1 rotor yielded an 8.7%, 7.0%, and 5.2% C_{PMax} improvement when tested at Reynolds numbers 73,000, 86,000, and 99,000, respectively. This condition may be caused by the valve's presence on the blade surface disrupting the flow-separation delay that normally occurs when the Reynolds number increases. Adding a single valve did not significantly affect the tip speed ratio corresponding with the C_{PMax}. The tip speed ratio range related to the C_{PMax} is 0.85 to 0.87 compared to SCNVs 0.84 to 0.86. A similar observation was made by Amiri and Anbarsooz (2019).

The rotor with a valve near the rotor tip (SCC1) consistently showed higher C_{PMax} than the other two for the three Reynolds numbers. This result is consistent with Amiri and Anbarsooz (2019) that the negative torque reduction by the valve at the tip has a greater impact because the air flows through the valve at a higher rate. In contrast, the rotor with a valve placed near the rotation axis (SCA1) produced the least improvement. A valve at this location is too close to the moment axis, resulting in the lowest negative torque reduction. Placing a valve near the rotation axis also disturbs the overlapping-gap flow that is supposed to energize the returning blade (Nakajima, Iio, and Ikeda, 2008). The overlapping-gap flow disturbance further reduces the effectiveness of the valve placed near the rotation axis. This finding shows a tradeoff between the positive and negative effects on each valve location.

Adding a single valve to the rotor did not change the trend of rotor C_T. Similar to the non-valve-aided rotor (SCNV), the C_{TMax} occurred at TSR=0.4 and decreased as the TSR increased. This applied to all three valve-aided rotors (SCA1, SCB1, and SCC1). The value of the C_{TMax} for SCC1 and SCB1 rotors increased, while the SCA1 rotor C_{TMax} remained close to the SCNV. Similar to the C_P result, the magnitude of C_{TMax} improvement decreased as the Reynolds number increased. A comparison of the result between the present study and the works of Amiri and Anbarsooz (2019) and Saha, Thotla, and Maity (2008) can be found in Table 3.

Table 3 Result comparison for studies on Savonius rotor aided with a single valve

Author	Valve shape	Valve location	Valve OAR	Reynolds Number	C_{PMax}	TSR for C_{TMax}
Saha, Thotla, and Maity (2008)	Slot	Center	Not specified	148,000 (estimated)	0.310	Not specified
Amiri and Anbarsooz (2019)	Rectangular	Center	0.33	138,000 (estimated)	0.116	0.55
The present study	Circular	Center	0.02	73,000	0.199	0.87

3.3. Effect of Valve Opening Area Ratio on the Rotor Performance

The valve opening area ratio was varied between 0.02 and 0.06 by increasing the number of valves with the same diameter. A total of six multi-valve rotors (SCA2, SCA3, SCB2, SCB3, SCC2, and SCC3) were made and tested in this study. The results showed a similar trend for the three-valve locations. Therefore, the study discussed the results mainly from SCC1, SCC2, and SCC3, with the valve at the tip. Figures 6a and 6b illustrate the effect of OAR on the SCC rotor C_P and C_T at the same Reynolds number of 73,000, while Table 4 summarizes the overall experiment result.

Figures 6a and 6b show that the rotors' performance coefficient decreases as the valve OAR increases. The C_{PMax} at Re=73,000 for SCC1, SCC2, and SCC3 is 0.199, 0192, and 0.187, respectively. The C_{TMax} for SCC1, SCC2, and SCC3 is 0.302, 0.291, and 0.284, respectively. Table 4 shows that these C_{PMax} and C_{TMax} downward trends can be observed in all three

valve locations and for all Reynolds numbers. This result indicates that the amplification of positive effects from increasing OAR, such as negative torque reduction, is weaker than that of negative effects. The design and working mechanism of the hinge-type valve may contribute to the reduced performance. The thin synthetic-leather fabric used as the valve material could be affected by the airflow condition and lifted open when unexpected.
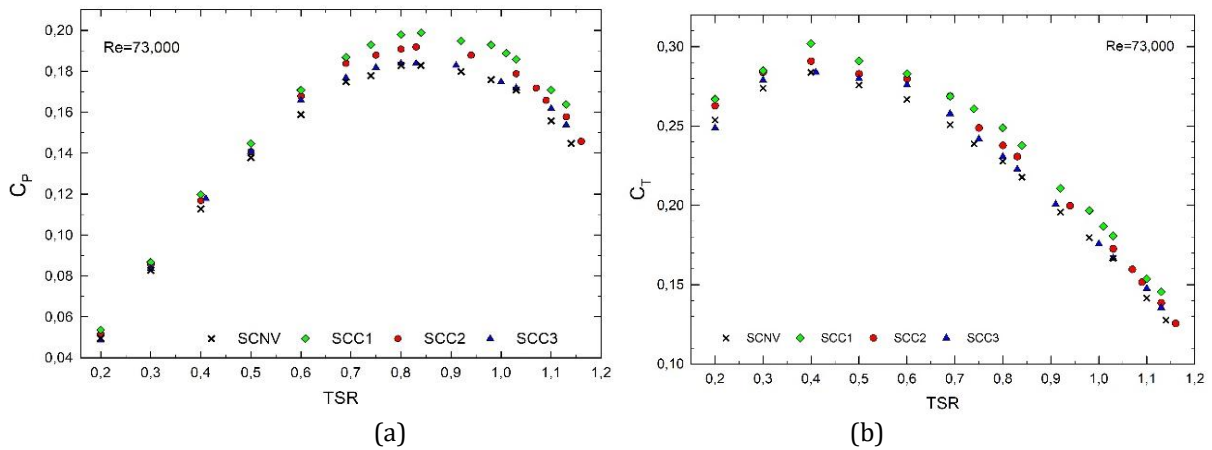

(a)   (b)

Figure 6 The effect of valve locations on SCNV, SCC1, SCC2, and SCC3 rotor (a) C_P vs TSR at Re=73,000; (b) C_T vs TSR at Re=73,000

Figure 7 shows the opening of all valves at returning and advancing blade side for the SCC3 rotor at 150º relative to the incoming wind. Opening the valves at the advancing side reduces the blade surface pushed by the wind, lowering the net torque value. This phenomenon is also observed with SCC1 and SCC2. Furthermore, increasing the OAR (number of valves) near the rotation axis has further disturbed the overlapping-gap flow, which cannot be compensated by the negative torque reduction effect. Figure 8 shows the plot for valve-aided rotors' C_{Pmax} improvement over the SCNV.

Table 4 Experiments result in summary

| Parameter	Reynolds Number = 73,000									
	SCNV	SCA1	SCA2	SCA3	SCB1	SCB2	SCB3	SCC1	SCC2	SCC3
C_{PMax}	0.183	0.191	0.187	0.182	0.198	0.191	0.185	0.199	0.192	0.187
TSR at C_{PMax}	0.85	0.86	0.87	0.86	0.86	0.87	0.86	0.87	0.86	0.85
C_{TMax}	0.284	0.284	0.276	0.272	0.293	0.282	0.275	0.302	0.291	0.284
Parameter	Reynolds Number = 86,000									
	SCNV	SCA1	SCA2	SCA3	SCB1	SCB2	SCB3	SCC1	SCC2	SCC3
C_{PMax}	0.200	0.206	0.199	0.195	0.211	0.203	0.199	0.214	0.207	0.202
TSR at C_{PMax}	0.84	0.86	0.85	0.86	0.85	0.85	0.86	0.87	0.86	0.85
C_{TMax}	0.304	0.303	0.290	0.281	0.314	0.300	0.287	0.320	0.314	0.306
Parameter	Reynolds Number = 99,000									
	SCNV	SCA1	SCA2	SCA3	SCB1	SCB2	SCB3	SCC1	SCC2	SCC3
C_{PMax}	0.210	0.215	0.208	0.205	0.219	0.211	0.208	0.221	0.214	0.210
TSR at C_{PMax}	0.84	0.85	0.84	0.85	0.86	0.85	0.85	0.86	0.84	0.83
C_{TMax}	0.323	0.316	0.299	0.291	0.327	0.306	0.302	0.335	0.329	0.326
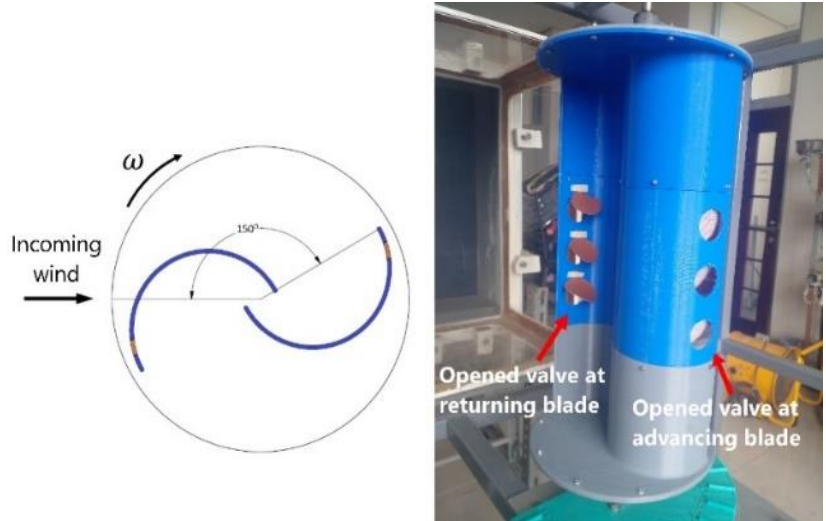
Figure 7 All valves on advancing and returning blades are open for the SCC3 rotor at a 150⁰ angle relative to the incoming wind
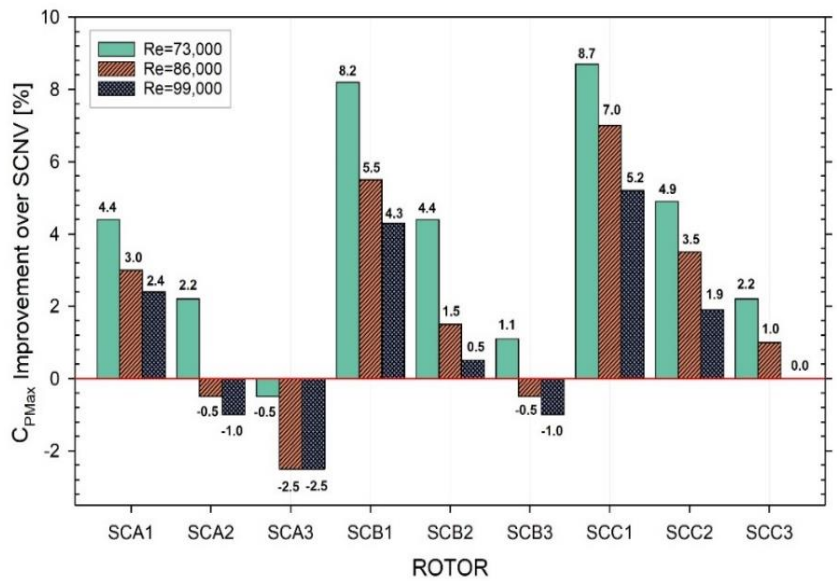

Figure 8 Summary of valve-aided rotors C_{Pmax} improvement over the SCNV rotor

4. Conclusions

The study aimed to compare the performance of conventional and valve-aided Savonius wind rotors with semi-circular blades by varying valve locations, OAR, and Reynolds numbers. Results indicated that rotor power and torque coefficient increased with Reynolds numbers. For all Reynolds numbers and OAR values, rotors with valves at the rotor tip outperformed those in other locations. Additionally, rotor performance decreased as valve OAR increased due to coexisting adverse effects like flow disruption alongside the beneficial effect of negative torque reduction. The highest C_{PMax} improvement of 8.7% was shown by the rotor with a single valve at the tip, with a C_{PMax} of 0.199 at a tip speed ratio of 0.87. The augmentation of the Savonius rotor with valve addition improved the rotor performance while keeping all the intrinsic advantages intact. Therefore, a valve-assisted Savonius wind rotor can potentially enhance wind power generation in urban areas and sites with a low average wind speed.

Acknowledgments

References

Abdelaziz, K.R., Nawar, M.A.A., Ramadan, A., Attai, Y.A., Mohamed, M.H., 2022. Performance Investigation of a Savonius Rotor by Varying the Blade Arc Angles. *Ocean Engineering,* Volume 260, p. 112054. https://doi.org/10.1016/j.oceaneng.2022.112054

Akwa, J.V., Vielmo, H.A., Petry, A.P., 2012. A Review on the Performance of Savonius wind Turbines. *Renewable and Sustainable Energy Reviews,* Volume 16(5), pp. 3054–3064. https://doi.org/10.1016/J.RSER.2012.02.056

Alom, N., Borah, B., Saha, U.K., 2018. An Insight into the Drag and Lift Characteristics of Modified Bach and Benesh Profiles of Savonius Rotor. *Energy Procedia,* Volume 144, pp. 50–56. https://doi.org/10.1016/j.egypro.2018.06.007

Alom, N., Saha, U.K., 2017. Arriving at the optimum overlap ratio for an elliptical-bladed savonius rotor. *Proceedings of the ASME Turbo Expo*, Volume 9, pp. 1–10. https://doi.org/10.1115/GT2017-64137

Amiri, M., Anbarsooz, M., 2019. Improving the Energy Conversion Efficiency of a Savonius Rotor Using Automatic Valves*. Journal of Solar Energy Engineering,* Volume 141(3), p. 031017. https://doi.org/10.1115/1.4042828

Banerjee, A., 2019. Performance and flow analysis of an elliptic bladed Savonius-style wind turbine. *Journal of Renewable and Sustainable Energy*, Volume 11(3), p. 033307. https://doi.org/10.1063/1.5097571

Borzuei, D., Moosavian, S.F., Farajollahi, M., 2021. On the Performance Enhancement of the Three-Blade Savonius Wind Turbine Implementing Opening Valve. *Journal of Energy Resources Technology,* Volume 143(5), p. 051301. https://doi.org/10.1115/1.4049460

Cho, K.-P., Jeong, S.-H., Sari, D.P., 2011. Harvesting Wind Energy from Aerodynamic Design for Building Integrated Wind Turbines. *International Journal of Technology,* Volume 2(3), pp. 189–198. https://doi.org/10.14716/ijtech.v2i3.65

Cuevas-Carvajal, N., Cortes-Ramirez, J.S., Norato, J.A., Hernandez, C., Montoya-Vallejo, M.F., 2022. Effect of Geometrical Parameters on the Performance of Conventional Savonius VAWT: A Review. *Renewable and Sustainable Energy Reviews,* Volume 161, p. 112314. https://doi.org/10.1016/J.RSER.2022.112314

Dinh Le, A., Minh, B.D., Trinh, C.D., 2022. High Efficiency Energy Harvesting Using a Savonius Turbine with Multicurve and Auxiliary Blade. *Journal of Fluids Engineering,* Volume 144(11), p. 111207. https://doi.org/10.1115/1.4054705

El-Askary, W.A., Nasef, M.H., AbdEL-hamid, A.A., Gad, H.E., 2015. Harvesting Wind Energy for Improving Performance of Savonius Rotor. *Journal of Wind Engineering and Industrial Aerodynamics,* Volume 139, pp. 8–15. https://doi.org/10.1016/j.jweia.2015.01.003

Elmekawy, A.M.N., Saeed, H.A.H., Kassab, S. Z., 2021. Performance Enhancement of Savonius Wind Turbine by Blade Shape and Twisted Angle Modifications*. In:* Proceedings of the Institution of Mechanical Engineers, Part A: Journal of Power and Energy, Volume 235(6), pp. 1487–1500. https://doi.org/10.1177/0957650920987942

Ferrari, G., Federici, D., Schito, P., Inzoli, F., Mereu, R., 2017. CFD study of Savonius wind turbine: 3D model validation and parametric analysis. *Renewable Energy*, Volume 105, pp. 722–734. https://doi.org/10.1016/j.renene.2016.12.077

Gonçalves, A.N.C., Pereira, J.M.C., Sousa, J.M.M., 2022. Passive Control of Dynamic Stall in a H-Darrieus Vertical Axis Wind Turbine using Blade Leading-Edge Protuberances. *Applied Energy*, Volume 324, p. 119700. https://doi.org/10.1016/j.apenergy.2022.119700

Intergovernmental Panel on Climate Change (IPCC), 2022. *Summary for Policymakers.* Report in Climate Change 2022: Impacts, Adaptation and Vulnerability, Contribution of Working Group II to the Sixth Assessment Report of the Intergovernmental Panel on Climate Change, IPCC, New York, USA. https://doi.org/10.1017/9781009325844.001

Ishugah, T.F., Li, Y., Wang, R.Z., Kiplagat, J.K., 2014. Advances in Wind Energy Resource Exploitation in Urban Environment: A Review. *Renewable and Sustainable Energy Reviews,* Volume 37, pp. 613–626. https://doi.org/10.1016/j.rser.2014.05.053

Kamoji, M.A., Kedare, S.B., Prabhu, S.V., 2009. Experimental Investigations on Single Stage Modified Savonius Rotor. *Applied Energy,* Volume 86(7–8), pp. 1064–1073. https://doi.org/10.1016/J.APENERGY.2008.09.019

Krasniqi, G., Dimitrieska, C., Lajqi, S., 2022. Wind Energy Potential in Urban Area: Case Study Prishtina. *International Journal of Technology,* Volume 13(3), pp. 458–472. https://doi.org/10.14716/ijtech.v13i3.5323

Kumar, R., Raahemifar, K., Fung, A.S., 2018. A Critical Review of Vertical Axis Wind Turbines for Urban Applications. *Renewable and Sustainable Energy Reviews*, Volume 89, pp. 281–291. https://doi.org/10.1016/j.rser.2018.03.033

Le, A.D., Minh Duc, B., van Hoang, T., The Tran, H., 2022. Modified Savonius Wind Turbine for Wind Energy Harvesting in Urban Environments. *Journal of Fluids Engineering,* Volume 144(8), p. 081501. https://doi.org/10.1115/1.4053619

Mahmoud, N.H., El-Haroun, A.A., Wahba, E., Nasef, M.H., 2012. An Experimental Study on Improvement of Savonius Rotor Performance. *Alexandria Engineering Journal,* Volume 51(1), pp. 19–25. https://doi.org/10.1016/J.AEJ.2012.07.003

Mao, Z., Yang, G., Zhang, T., Tian, W., 2020. Aerodynamic performance analysis of a building-integrated Savonius turbine. *Energies*, Volume 13(10), p. 2636. https://doi.org/10.3390/en13102636

Mohamed, M.H., Janiga, G., Pap, E., Thèvenin, D., 2010. Optimization of Savonius Turbines using an Obstacle Shielding the Returning Blade. *Renewable Energy,* Volume 35(11), pp. 2618–2626. https://doi.org/10.1016/j.renene.2010.04.007

Nakajima, M., Iio, S., Ikeda, T., 2008. Performance of Double-step Savonius Rotor for Environmentally Friendly Hydraulic Turbine. *Journal of Fluid Science and Technology,* Volume 3(3), pp. 410–419. https://doi.org/10.1299/jfst.3.410

Nimvari, M.E., Fatahian, H., Fatahian, E., 2020. Performance Improvement of a Savonius Vertical Axis Wind Turbine using a Porous Deflector. *Energy Conversion and Management*, Volume 220, p. 113062. https://doi.org/10.1016/j.enconman.2020.113062

Nur, T., Siregar, M., 2020. Two-Steps Slotting Method in Magnet Edge of PMG for Wind Energy Harvesting. *International Journal of Technology,* Volume 11(7), pp. 1442–1450. https://doi.org/10.14716/ijtech.v11i7.4554

Rajkumar, M.J., Saha, U.K., 2006. Valve-Aided Twisted Savonius Rotor. *Wind Engineering,* Volume 30(3), pp. 243–254. https://doi.org/10.1260/030952406778606269

Renewable Energy Policy Network for the 21st Century (REN21), 2019. *Renewables 2019 Global Status Report*. Renewable Energy Policy Network for the 21st Century, REN21 Secretariat, Paris, France

Roy, S., Saha, U.K., 2013. Computational Study to Assess the Influence of Overlap Ratio on Static Torque Characteristics of a Vertical Axis Wind Turbine. *Procedia Engineering*, Volume 51, pp. 694–702. https://doi.org/10.1016/J.PROENG.2013.01.099

Roy, S., Saha, U.K., 2015. Wind tunnel experiments of a newly developed two-bladed Savonius-style wind turbine. *Applied Energy*, Volume 137, pp. 117–125. https://doi.org/10.1016/j.apenergy.2014.10.022

Saad, A.S., El-Sharkawy, I.I., Ookawara, S., Ahmed, M., 2020. Performance Enhancement of Twisted-Bladed Savonius Vertical Axis Wind Turbines. *Energy Conversion and Management,* Volume 209, p. 112673. https://doi.org/10.1016/j.enconman.2020.112673

Saad, A.S., Ookawara, S., Ahmed, M., 2022. Influence of Varying the Stage Aspect Ratio on the Performance of Multi-Stage Savonius Wind Rotors. *Journal of Energy Resources Technology,* Volume 144(1), p. 011301. https://doi.org/10.1115/1.4050876/1107060.

Saha, U.K., Thotla, S., Maity, D., 2008. Optimum Design Configuration of Savonius Rotor Through Wind Tunnel Experiments. *Journal of Wind Engineering and Industrial Aerodynamics,* Volume 96(8–9), pp. 1359–1375. https://doi.org/10.1016/J.JWEIA.2008.03.005

Torresi, M., de Benedittis, F.A., Fortunato, B., Camporeale, S.M., 2014. Performance and Flow Field Evaluation of a Savonius Rotor Tested in a Wind Tunnel. *Energy Procedia,* Volume 45, pp. 207–216. https://doi.org/10.1016/J.EGYPRO.2014.01.023

Van Bussel, G.J.W., Mertens, S., Polinder, H., Sidler, H.F.A., 2004. The Development of Turby, A Small Vawt for the Built Environment. *In:* Proceedings of the Global Windpower 2004 Conference and Exhibition, pp. 1–10

Wheeler, A., Ganji, A., 2009. *Introduction to Engineering Experimentation.* 3rd Edition. USA: Pearson

Wiser, R., Rand, J., Seel, J., Beiter, P., Baker, E., Lantz, E., Gilman, P., 2021. Expert Elicitation Survey Predicts 37% to 49% Declines in Wind Energy Costs by 2050. *Nature Energy,* Volume 6(5), pp. 555–565. https://doi.org/10.1038/s41560-021-00810-z